REDUCTION OF PEAK SAR IN HUMAN HEAD FOR HANDSET APPLICATIONS WITH RESISTIVE SHEETS (R-CARDS)

H.-H. Chou

Communication Research Center
Yuan Ze University
Chungli 320, Taiwan

H.-T. Hsu, H.-T. Chou, K.-H. Liu, and F.-Y. Kuo

Department of Communications Engineering
Communication Research Center
Yuan Ze University
Chungli 320, Taiwan

Abstract—In this paper, reduction of peak specific absorption rate (SAR) for handsets with monopole type antenna through R-cards is investigated. While the numerical analysis was performed using finite integration in time domain (FIT), real measurement has been made to validate the simulation results. Both the simulation and measurement results revealed that a minimum SAR Reduction Factor (SRF) of 60% was achieved. The good agreement between the simulation and measurement results has evidenced the effectiveness of the proposed approach for SAR reduction in human head for handset applications.

1. INTRODUCTION

With the rapid growth in the use of cellular phones, public concern regarding the exposure of human head to electromagnetic radiation has increased. The specific absorption rate (SAR) is a defined figure of merit to evaluate the power absorbed by biological tissue. For mobile phone compliance, the SAR value must not exceed the exposure limits [1, 2]. For example, the SAR limit specified in IEEE C95.1 : 1999 is $1.6 \, \text{W/kg}$ in a $1 \, \text{g}$ averaging mass while that specified in ICNIRP guidelines is $2 \, \text{W/kg}$ in a $10 \, \text{g}$ averaging mass [3].

Corresponding author: H.-T. Hsu (htbeckhsu@saturn.yzu.edu.tw).

The regulation in SAR has been harmonized to 10 g with a limit of 2 W/kg specified in IEEE C95.1 : 2005 with the major difference discussed in detail in [4]. In general, the SAR value is influenced by various parameters such as antenna positions relative to the human body, radiation patterns of the antenna, radiated power, and antenna types [5].

Over the years, lots of attentions have been paid to the analysis of SAR in human head due to the complexity and large scale involved in this kind of problems [6–11]. Recently, research efforts have been devoted to the reduction of peak SAR in human head for handset applications. In [12], a ferrite sheet was adopted as protection attachment between the antenna and the head. A reduction over 13% for the spatial peak SAR over 1 g averaging was achieved. Experimental study on the effects of attaching conductive materials for SAR reduction was presented [13]. It was concluded that the position of shielding played an important role in the reduction effectiveness. Metamaterials composed of an array of split ring resonators (SRR) were applied to the reduction of SAR in [14]. With proper design and arrangement, stop bands at desired cellular frequencies could be obtained to notch out the radiated power. Highly directive antennas were also utilized for SAR reduction [15].

In practical situations, the ease-of-implementaion also plays a critical role especially for handset applications. Furthermore, adoption of highly-directive antennas certainly causes degradations in signal reception which may have major impact on system performance. The main purpose of this paper is to propose an effective approach using R-cards for peak SAR reduction. The effectiveness of SAR reduction will be emphasized together with the ease of practical implementation. R-cards are resistive sheets that possess interesting electromagnetic properties and capable of either blocking or attenuating electromagnetic power through impedance transformation [16]. Since technology advancement has made it possible to realize any impedance level at very low cost, adoption of R-cards in handset applications becomes feasible especially in terms of production cost. Optimum values and positions for R-cards implementation will be investigated through numerical simulations followed by experimental validation.

This paper is organized as follows. Section 2 describes the numerical analysis of the handset together with the SAM phantom head. Finite integration in time-domain (FITD) method is adopted with certain meshing techniques for fast and accurate analysis [16, 17]. Simulation results will be summarized in Section 3. Experimental validation based on the analyzed results is included in Section 4

followed by the conclusion in Section 5.

2. SIMULATION MODEL AND NUMERICAL TECHNIQUES

2.1. Model Description

Figure 1 shows the simulation model which includes the handset with monopole type of antenna and the SAM phantom head provided by CST Microwave Studio$^{\circledR}$ (CST MWS) [18]. Complete handset model composed of the circuit board, LCD display, keypad, battery and housing was used for simulation. The relative permittivity and conductivity of individual components were set to comply with industrial standards. In addition, definitions in [19] were adopted for material parameters involved in the SAM phantom head. In order to accurately characterize the performance over broad frequency range, dispersive models for all the dielectrics were adopted during the simulation. Fig. 2 shows the dispersive permittivity of the liquid in SAM phantom head for simulation.

The electrical properties of materials used for simulation are listed in Table 1. Monopole type antenna constructed in a helical sense operating at 1800 MHz for GSM application was used in the simulation model. In order to obtain good geometry approximation for such helical structure, conventional meshing scheme used in FDTD method usually requires large number of hexahedrons which in turn makes it extremely challenging to get converged results within reasonable simulation time.

Figure 1. Complete model used for simulation including handset and SAM phantom head.
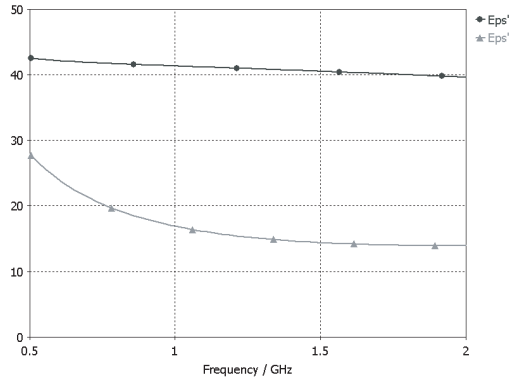
Figure 2. Dispersive permittivity of the liquid in SAM phantom head for simulation.

Table 1. Electrical properties of materials used for simulation.

Phone Materials	ε_r	σ (S/m)
Circuit Board	4.4	0.05
Housing Plastic	2.5	0.005
LCD Display	3.0	0.02
Rubber	2.5	0.005
SAM Phantom Head	ε_r	σ (S/m)
Shell	3.7	0.0016
Liquid @ 1.8 GHz	40	1.42

Three different scenarios, denoted as cases A, B, and C, respectively in Fig. 3, were used to study the effectiveness of SAR reduction. The main difference for the three cases is in the relative location for R-card implementation. In case A, the R-card covered the keypad area. In case B, the R-card was attached on top of the LCD display and was extended beyond the antenna feed. As for case C, the R-card was attached in a manner to wrap around the monopole antenna. The surface impedance of the R-card is related to the conductivity and thickness as:

$$Z = \frac{1}{\sigma t} \tag{1}$$

with σ being the conductivity and t the thickness of the R-card. In our simulation models, R-cards with impedance values of $5\,\Omega$, $40\,\Omega$, $250\,\Omega$, and $1150\,\Omega$ were included to investigate the impact on the SAR

reduction.

(a)   (b)   (c)
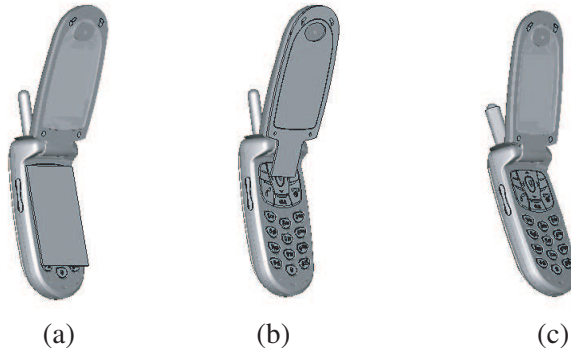
Figure 3. Three locations for R-card implementation, (a) case A: R-card covering keypad area, (b) case B: R-card covering LCD display and extending beyond antenna feed, and (c) R-card wrapping around the monopole antenna.

2.2. Numerical Technique

CST MWS, which adopted finite integral time-domain technique (FITD) proposed by Weiland in 1976 [20], was used as the main simulation tool. In combination of the perfect boundary approximation (PBA$^{\circledR}$) and thin sheet technique (TST$^{\circledR}$), significant improvement in geometry approximation with computation speed is achieved yielding highly accurate results. Non-uniform meshing scheme was adopted so that major computation effort was devoted to regions along the inhomogeneous boundaries for fast and accurate analysis. Fig. 4 shows the mesh view for two cut planes of the complete model indicating the area with denser meshing along the inhomogeneous boundaries. The minimum and maximum mesh sizes were 0.3 mm and 18 mm, respectively. A total of 546,459 mesh cells were generated for the complete model, and the simulation time was 823 seconds (including mesh generation) for each run on an Intel$^{\circledR}$ Core^{TM} 2 Duo T9300 2.5 GHz CPU with 4 GB RAM system.

The analysis workflow started from the design of antenna with complete handset model in free space. The antenna was designed such that the S_{11} response was less than -10 dB over the frequency band of interest. SAM phantom head was then included for SAR calculation
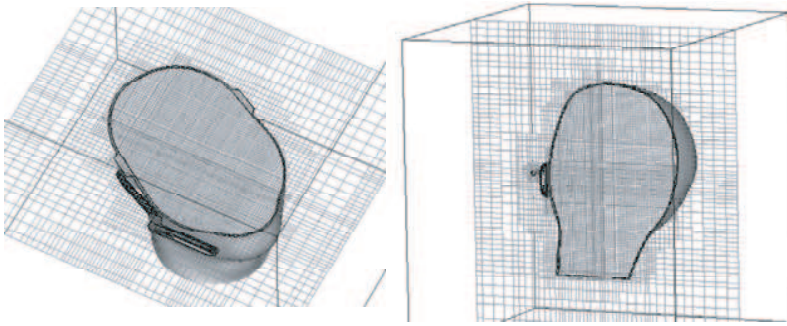
Figure 4. Mesh view for two cut planes of the complete model showing the non-uniform meshing scheme adopted for simulation.

using the standard definition as

$$SAR = \frac{\sigma}{2\rho}E^2 \qquad (2)$$

where E is the induced electric field (V/m); ρ is the density of the tissue (kg/m^3) and σ is the conductivity of the tissue (S/m). The corresponding SAR values averaged over 1 g and 10 g of tissue in the head were denoted as $SAR_{1\,g}$ and $SAR_{10\,g}$, respectively. These values were used as a benchmark to evaluate the effectiveness in peak SAR reduction.

To quantify the effectiveness for peak SAR reduction, the SAR Reduction Factor (SRF), defined as the ratio of difference in SAR to the benchmark value [5], was adopted and expressed as

$$SRF = \frac{\left| SAR_{1\,g(10\,g)}^{R(Z)} - SAR_{1\,g(10\,g)} \right|}{SAR_{1\,g(10\,g)}} \times 100\%. \qquad (3)$$

In the above equation, $SAR_{1\,g(10\,g)}^{R(Z)}$ denotes the peak SAR value with implementation of ZΩ R-card averaged over 1 g (10 g) tissue mass, and $SAR_{1\,g(10\,g)}$ is the corresponding benchmark value without R-card. Introduction of the R-card will certainly detune the antenna match of the benchmark case which in turn influences the radiated power level under the same excitation condition. In order to have a fair comparison and avoid possible ambiguities caused by antenna mismatch, the actual radiated power out of the antenna defined in the equation below was set to be 125 mW for all the cases under study. With such constraint, scale or re-normalization of SAR levels are no longer necessary, and

the results are more realistic to the practical situation.

$$P_{radiated} = \left(1 - |S_{11}|^2\right) P_{stimulated} \tag{4}$$

S-parameter Magnitude in dB
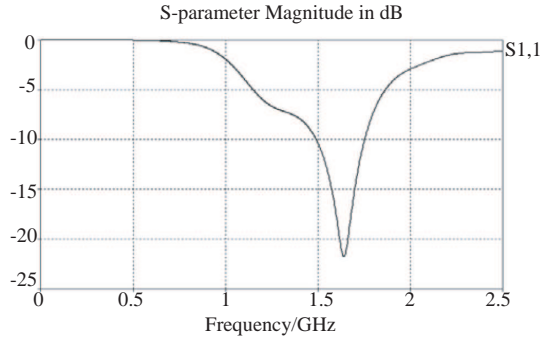
Figure 5. Simulated S_{11} of the complete model including handset and SAM phantom head showing proper operation of the antenna.

Table 2. Simulated Peak SAR value and the SRF averaging over 1 g tissue

	Peak SAR Value			SRF (%)		
	Case A	Case B	Case C	Case A	Case B	Case C
$SAR_{1\,g}^{R(5)}$	1.07	0.51	0.983	4.762	54.606	12.506
$SAR_{1\,g}^{R(40)}$	0.977	0.585	0.759	13.040	47.931	32.443
$SAR_{1\,g}^{R(250)}$	1.1	0.82	0.463	2.092	27.014	58.789
$SAR_{1\,g}^{R(1150)}$	1.123	0.926	0.556	0.045	17.579	50.512

Table 3. Simulated Peak SAR value and the SRF averaging over 10 g tissue.

	Peak SAR Value			SRF (%)		
	Case A	Case B	Case C	Case A	Case B	Case C
$SAR_{10\,g}^{R(5)}$	0.731	0.24	0.648	1.163	67.550	12.385
$SAR_{10\,g}^{R(40)}$	0.638	0.36	0.5	13.737	51.325	32.396
$SAR_{10\,g}^{R(250)}$	0.723	0.508	0.305	2.244	31.314	58.761
$SAR_{10\,g}^{R(1150)}$	0.739	0.574	0.366	0.081	22.390	50.514

x-z cut   y-z cut
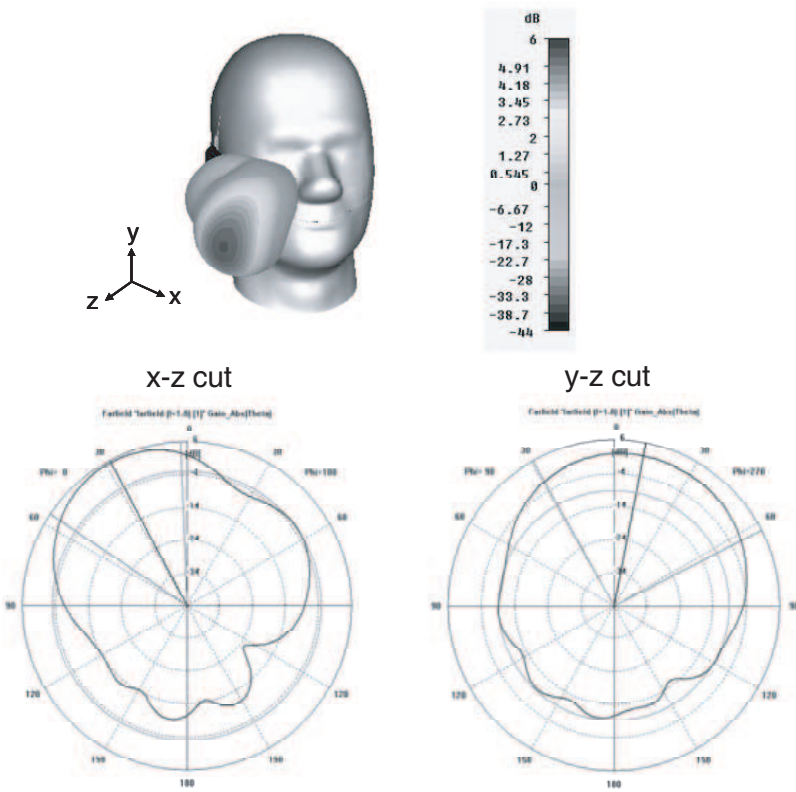
Figure 6. Simulated 3D farfield radiation patterns with polar plots at x-z and y-z cuts, all at 1800 MHz.
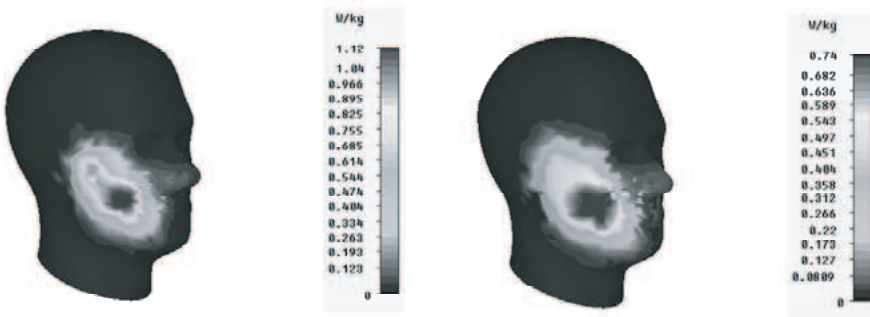
Figure 7. SAR distribution for the case of 1 g (left) and 10 g (right).

3. SIMULATION RESULTS

Figure 5 shows the simulated S_{11} of the complete model including handset and the SAM phantom head. The excitation port is located at the feed to the monopole antenna. A total number of 89,412 mesh cells was used for simulation, and total simulation time elapsed was 7 minutes and 2 seconds on 2.5 GHz dual core CPU system with 4 GB RAM. It is observed that even though the SAM phantom head may have certain detuning effect on the return loss, the antenna is operating in the band of interest.

The 3D farfield radiation patterns at 1800 MHz together with the polar plots at two corresponding cuts are included in Fig. 6. Fig. 7 shows the SAR distribution for the cases of 1 g and 10 g, respectively. The benchmark value of the peak $SAR_{1\,g}$ is calculated to be 1.12 W/kg, and that of the $SAR_{10\,g}$ is 0.74 W/kg, respectively. Tables 2 and 3 summarize the simulated peak SAR values and the corresponding SAR reduction factor (SRF) compared with the benchmark values at 1800 MHz. It is clear that the application of R-cards does have effect in the reduction of peak SAR values. Moreover, the locations and impedance levels for R-cards have different impact on the effectiveness of peak SAR reduction. Maximum SRF for 1 g and 10 g cases both occurred at case B with 5 Ω R-card applied.

As mentioned in previous sections, the ultimate goal for R-card implementation is to have maximum SRF while not deteriorating too much the antenna performance. Thus, investigations of the antenna performance with the existence of R-cards are necessary. Fig. 8 shows the simulated return loss of the antenna with the existence of R-cards at various impedance levels. It is clearly observed that inclusion of R-cards has certain impact on the return loss of the antenna. Such impact would have certain degradation in the power delivered which would cause ambiguities for SAR comparison. In our case, the effect of antenna mismatch has been taken into account to avoid the possible ambiguities.

Figure 9 shows the farfield radiation patterns with the inclusion of R-cards. Three different cases with all combinations of impedance levels at the y-z and x-z cuts are plotted. It is observed that the radiation patterns are not influenced too much with the implementation of the R-cards for cases A and B. For case C, however, the degradation in the radiated antenna gain is more pronounced for R-cards with higher impedance levels. An almost 3 dB degradation in peak gain is observed for R-card with 1150 Ω impedance for case C. Apparently, in practical situation, implementation of R-card in the manner of case B such that the R-card covers the LCD display and
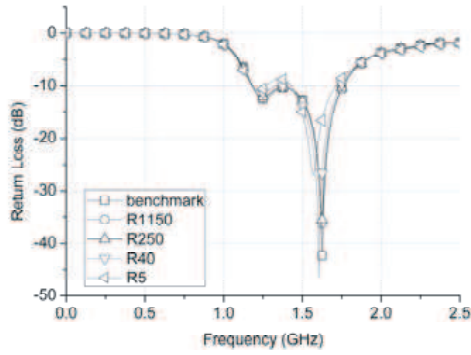
(a)
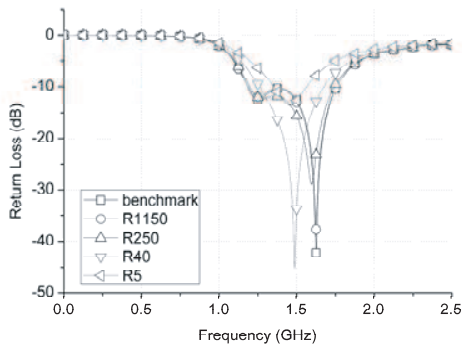
(b)
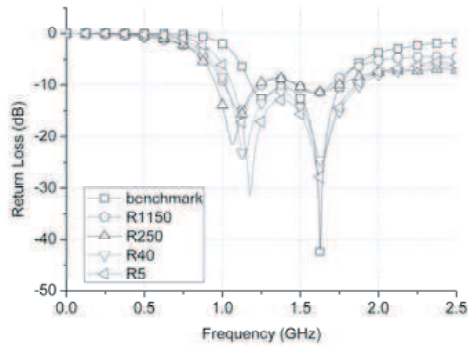
(c)

Figure 8. Effect of the R-card on the simulated return loss: (a) case A, (b) case B and (c) case C.

y-z cut   x-z cut

(a) Case A

y-z cut   x-z cut

(b) Case B

y-z cut   x-z cut
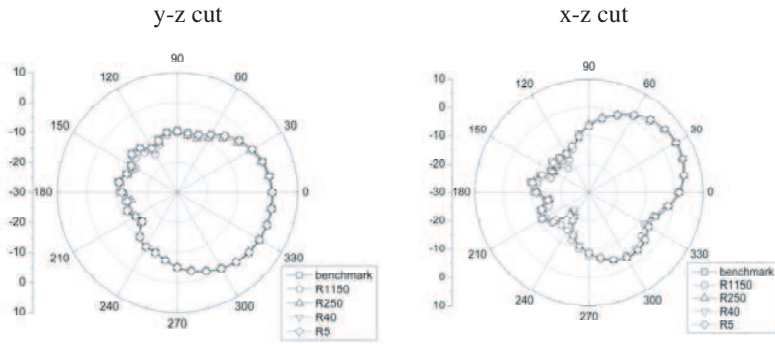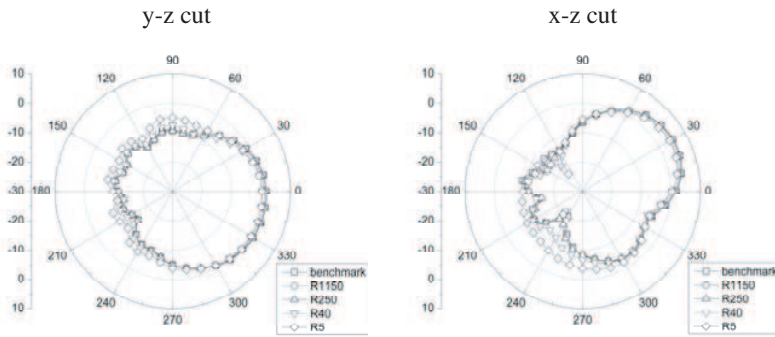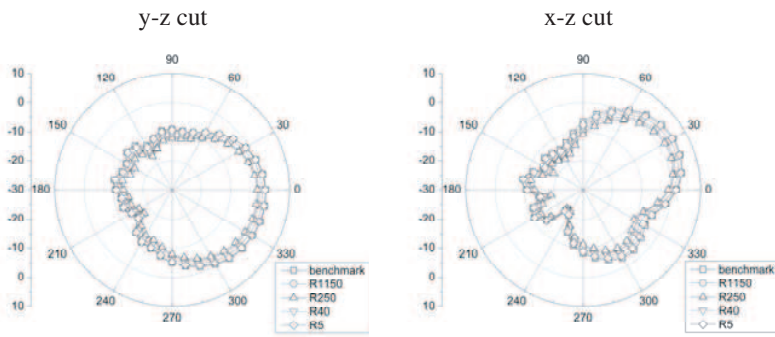
(c) Case C

Figure 9. Effect of the R-card on the simulated return loss: (a) case A, (b) case B and (c) case C.

extends beyond the antenna feed could be a favorable choice due to the ease of implementation.

4. EXPERIMENTAL VALIDATION

Experimental validation has been performed based on the analysis results from simulations presented in the previous section. The model of the handset used for measurement is Motorola$^{\circledR}$ V180 with the picture shown in Fig. 10, which is similar to the one used for simulation.

Figure 10. Photograph of Motorola$^{\circledR}$ V180 handset used for measurement.

For three dimensional SAR measurements, we used canonical cut system with Agilent N5230A vector network analyzer. The conceptual diagram of the measurement system is shown in Fig. 11. Fig. 12 shows the photograph for the real measurement where the handset is held against the SAM phantom head for SAR measurement. Anritsu 8820A system was used as the base station to maintain the communication link with the handset, and the channel was set at middle one.

Four different impedance levels of R-cards, 5 Ω, 36 Ω, 247 Ω, and 1150 Ω were attached to the handset in a manner similar to case B. Fig. 13 shows the SAR distribution on the selected planar cut of the SAM phantom head with 36 Ω R-card. The tabulated peak SRF values under different test conditions are also included. From the measurement results, it is clear that a very similar trend for peak SAR reduction is obtained compared to the simulation results. As for the difference in the absolute values of peak SAR, we believe that
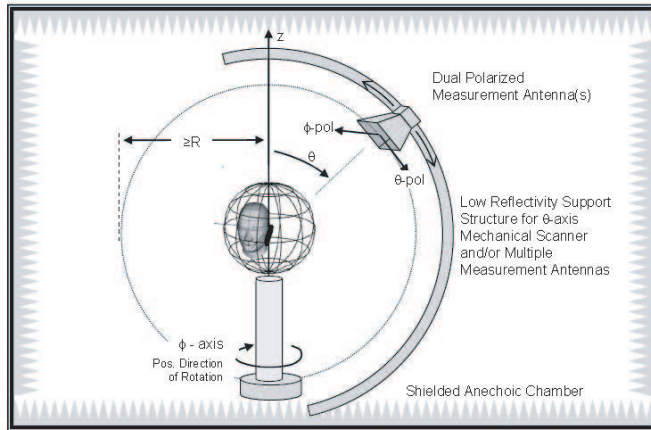
Figure 11. Conceptual diagram of the 3D canonical cut measurement system.
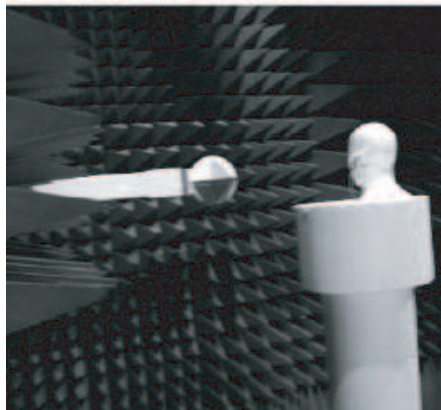
Figure 12. Photograph of the real measurement system including handset and SAM phantom head.

the power level adopted for simulation is different from the case for measurement. Practically, it may not be easy to make the two exact the same, especially when power control mechanism is on for real measurement. Finally, investigation of the R-card on the antenna gain over three different cuts was tested and plotted in Fig. 14. As observed, such implementation does not deteriorate the gain performance of the antenna which makes it attractive for practical implementation.
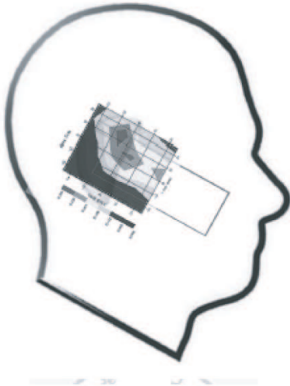
	Peak SAR Value		SRF (%)	
	1g	10g	1g	10g
No R-card	1.226	0.680	--	--
5Ω	0.455	0.275	62.8	59.5
36Ω	0.432	0.253	64.7	62.7
247Ω	0.679	0.393	44.6	42.2
1150Ω	0.872	0.552	28.8	18.8

Figure 13. SAR distribution on the selected planar cut of the SAM phantom head with $36\,\Omega$ R-card. The tabulated peak SAR values under different test conditions is also included.

	F-N	PA-5	PA-36	PA-247	PA-1150
X-Z	0	-4.876	-5.685	-2.971	-2.017
Y-Z	0	-4.126	-5.084	-2.614	-1.684
X-Y	0	-4.625	-5.529	-2.799	-1.806
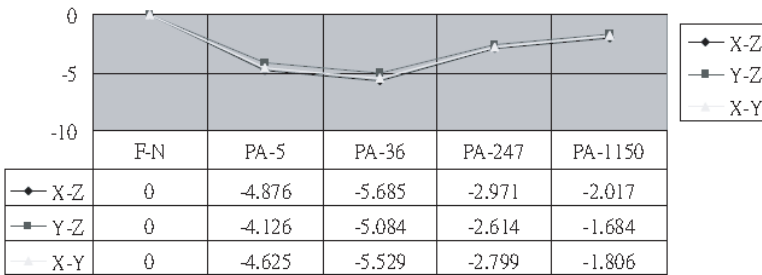
Figure 14. Measured antenna gain on three different cuts with various impedance levels of R-card implementation showing very little impact of the R-card on the antenna performance.

5. CONCLUSION

Effect of the reduction in peak SAR for handset with monopole type antenna using R-card is investigated numerically and experimentally. The numerical analysis results using FIT technique suggest that implementation of R-card with low impedance levels in a sense to cover the antenna feed can effectively reduce the peak SAR value in the human head for both $1\,g$ and $10\,g$ cases. Such an observation has been validated experimentally, and a peak SAR reduction of over 60% has been achieved in real measurement. In addition to the effectiveness of peak SAR reduction, this approach has very little impact on the antenna performance while maintaining the advantage of ease for implementation.

REFERENCES

1. IEEE Standard for Safety Levels with Respect to Human Exposure to Radio Frequency Electromagnetic Fields, 3 kHz to 300 GHz, IEEE C95.1-1991, Institute of Electrical and Electronics Engineers, Inc., New York, 1992.

2. International Non-Ionizing Radiation Committee of the International Radiation Protection Association, "Guidelines on limits of exposure to radio frequency electromagnetic fields in the frequency range from 100 kHz to 300 GHz," *Health Phys.*, Vol. 54, No. 1, 115–123, 1988.

3. Fung, L. C., S. W. Leung, and K. H. Chan, "An investigation of the SAR reduction methods in mobile phone applications," *2002 IEEE International Symposium on EMC*, Vol. 2, 656–660, Aug. 2002.

4. Lin, J. C., "A new IEEE standard for safety levels with respect to human exposure to radio-frequency radiation," *IEEE Antennas and Propagation Magazine*, Vol. 48, No. 1, Feb. 2006.

5. Jung, M. and B. Lee, "SAR reduction for mobile phones based on analysis of EM absorbing material characteristics," *2003 IEEE International Symposium on Antennas and Propagation*, Vol. 2, 1017–1020, Jun. 2003.

6. Khalatbari, S., D. Sardari, A. A. Mirzaee, and H. A. Sadafi, "Calculating SAR in two models of the human head exposed to mobile phones radiations at 900 and 1800 MHz," *PIERS Online*, Vol. 2, No. 1, 104–109, 2006.

7. Hirata, A., K. Shirai, and O. Fujiwara, "On averaging mass of SAR correlating with temperature elevation due to a dipole antenna," *Progress In Electromagnetics Research*, PIER 84, 221–237, 2008.

8. Mahmoud, K. R., M. El-Adawy, S. M. M. Ibrahem, R. Bansal, and S. H. Zainud-Deen, "Investigating the interaction between a human head and a smart handset for 4 g mobile communication systems," *Progress In Electromagnetics Research C*, Vol. 2, 169–188, 2008.

9. Kouveliotis, N. K. and C. N. Capsalis, "Prediction of the SAR level induced in a dielectric sphere by a thin wire dipole antenna," *Progress In Electromagnetics Research*, PIER 80, 331–336, 2008.

10. Ebrahimi-Ganjeh, M. A. and A. R. Attari, "Interaction of dual band helical and pifa handset antennas with human head and hand," *Progress In Electromagnetics Research*, PIER 77, 225–242, 2007.

11. Kuo, L.-C., Y.-C. Kan, and H.-R. Chuang, "Analysis of a

900/1800-MHz dual-band gap loop antenna on a handset with proximate head and hand model," *Journal of Electromagnetic Waves and Applications*, Vol. 21, No. 1, 107–122, 2007.

12. Wang, J. and O. Fujiwara, "Reduction of electromagnetic absorption in the human head for portable telephones by a ferrite sheet attachment," *IEICE Transactions on Communications*, Vol. E80-B, No. 12, 1810–1815, Dec. 1997.

13. Fung, L. C., S. W. Leung, and K. H. Chan, "Experimental study of SAR reduction on commercial products and shielding materials in mobile phone applications," *Microwave and Optical Technology Letters*, Vol. 36, No. 6, 419–422, Mar. 2003.

14. Hwang, J.-N. and F.-C. Chen, "Reduction of the peak SAR in the human head with metamaterials," *IEEE Trans. Antennas Propagat.*, Vol. 54, No. 12, 3763–3769, Dec. 2006.

15. Kim, K. W. and Y. Rahmat-Samii, "Handset antennas and humans at Ka-band: The importance of directional antennas," *IEEE Trans. Antennas Propagat.*, Vol. 46, No. 6, 949–950, Jun. 1998.

16. Krietenstein, B., R. Schuhmann, P. Thoma, and T. Weiand, "The perfect boundary approximation technique facing the big challenge of high precision field computation," *XIX International Linear Accelerator Conference (LINAC 98)*, Chicago, 1998.

17. Qi, N., M. Zhang, T. Wittig, and A. Prokop, "Application of CST time domain algorithm in the electromagnetic simulation standard of the SAR for mobile phone," *International Conference on Microwave and Millimeter Wave Technology, ICMMT 2008*, Vol. 4, 1717–1720, Apr. 2008.

18. CST Microwave Studio Suite 2009 User's Manual, www.cst.com.

19. FCC, "Evaluating compliance with FCC guidelines for human exposure to radiofrequency electromagnetic fields," Supplement C to OET Bulletin 65, Washington, DC, FCC, Jun. 2001.

20. Weiland, T., "A discretization method for the solution of maxwell's equations for six-component fields," *Electronics and Communication (AEÜ)*, Vol. 31, 116, 1977.